J Biomol NMR (2011) 51:329–337
DOI 10.1007/s10858-011-9560-y

ARTICLE

# Cys-Ph-TAHA: a lanthanide binding tag for RDC and PCS enhanced protein NMR

**Fabian Peters · Mitcheell Maestre-Martinez · Andrei Leonov · Lidija Kovačič · Stefan Becker · Rolf Boelens · Christian Griesinger**

Received: 29 March 2011 / Accepted: 11 August 2011 / Published online: 4 September 2011


**Abstract** Here we present Cys-Ph-TAHA, a new nonadentate lanthanide tag for the paramagnetic labelling of proteins. The tag can be easily synthesized and is stereochemically homogenous over a wide range of temperatures, yielding NMR spectra with a single set of peaks. Bound to ubiquitin, it induced large residual dipolar couplings and pseudocontact shifts that could be measured easily and agreed very well with the protein structure. We show that Cys-Ph-TAHA can be used to label large proteins that are biochemically challenging such as the Lac repressor in a 90 kDa ternary complex with DNA and inducer.

**Keywords** Lanthanides · Pseudocontact shifts · Residual dipolar couplings · Paramagnetic NMR

**Electronic supplementary material** The online version of this article (doi:10.1007/s10858-011-9560-y) contains supplementary material, which is available to authorized users.

F. Peters · M. Maestre-Martinez · A. Leonov · S. Becker · C. Griesinger (✉)
Department of NMR-Based Structural Biology, Max Planck Institute for Biophysical Chemistry, Am Fassberg 11, 37077 Göttingen, Germany
e-mail: cigr@nmr.mpibpc.mpg.de

L. Kovačič · R. Boelens
Bijvoet Center for Biomolecular Research, Department of NMR Spectroscopy, Utrecht University, Padualaan 8, 3584 CH Utrecht, The Netherlands

L. Kovačič
Department of Molecular and Biomedical Sciences, Jožef Stefan Institute, 1000 Ljubljana, Slovenia

## Introduction

NMR spectroscopy offers rich information for the study of structure and dynamics of biomolecules at atomic resolution. In addition to well established methods based on the measurement of diamagnetic parameters, NMR parameters induced by paramagnetism such as paramagnetic relaxation enhancement (PRE), pseudocontact shifts (PCSs), paramagnetically induced residual dipolar couplings (RDCs) and Curie-dipolar cross correlated relaxation provide complementary information and have recently attracted much attention (Tolman et al. 1995; Bertini and Luchinat 1999; Hus et al. 2000; Bertini et al. 2002; Kramer et al. 2004; Rodriguez-Castañeda et al. 2006; Otting 2008; Su and Otting 2010). The long-range nature of these interactions makes them especially valuable in providing a better description of non-covalent complexes. In addition, paramagnetic alignment allows for the study of domain motions by simply scaling the alignment tensor of a non-paramagnetic domain with respect to the alignment tensor of the paramagnetic one. (Lakomek et al. 2006; Lange et al. 2008; Lakomek et al. 2008; Xu et al. 2009).

Lanthanide ions, having the largest Curie-spin and anisotropic magnetic susceptibilities, are commonly used to induce the above-described paramagnetic effects. Lanthanides can be introduced into diamagnetic proteins either by the selective loading of a metal binding site of a metalloprotein (Allegrozzi et al. 2000; Bertini et al. 2003), or by site-specific attachment of a metal binding tag. In order to broaden the application of paramagnetic NMR parameters to diamagnetic molecules, existing tags can still be improved with respect to robustness, availability and comfort of use. Several different approaches concerning the design and the attachment of such tags to proteins have been reported in the past (Su and Otting 2010).

For example, lanthanide-binding peptides can be attached, or inserted into the sequence of a protein (Wöhnert et al. 2003; Nitz et al. 2004; Martin et al. 2007; Su et al. 2008a). The introduction of a lanthanide binding peptide into loop regions has been found to have a small effect on the overall structure of the protein (Barthelmes et al. 2011). However, even less invasive is the attachment of a small chemically synthesized tag via a disulfide bridge to a single solvent exposed cysteine residue. Many tags based on organic ligands like EDTA (Gaponenko et al. 2002; Ikegami et al. 2004; Leonov et al. 2005; Haberz et al. 2006), DPA (Su et al. 2008b; Man et al. 2010), DOTA (Keizers et al. 2007; Keizers et al. 2008; Häussinger et al. 2009), IDA (Swarbrick et al. 2011a) or NTA (Swarbrick et al. 2011b) have been developed to observe paramagnetic effects. So far, the largest RDCs obtained with paramagnetic tagging using a single cysteine residue have been reported with the DOTA-M8 and the IDA-based tag (Häussinger et al. 2009; Swarbrick et al. 2011a), while for two-point attachment even larger values have been measured by either using two NTA ligands (Swarbrick et al. 2011b) or by connecting the tag via two disulfide bridges (CLaNP-5, Keizers et al. 2008). Nevertheless, we decided to use a single cysteine residue for the attachment for two reasons: less a priori structural information is required to select the single mutation site and second the number of mutations is reduced to a minimum. We now introduce our new tag and discuss it in light of the performance of existing tags.

For the design of the Cys-Ph-TAHA tag (cysteinyl-phenyl-triaminohexaacetate, Fig. 1) the following requirements were taken into account: complex stability for different temperatures and pH values, completeness of the tagging reaction and avoidance of the formation of diastereomeric complexes which would give rise to more than one set of NMR signals due to different tensors induced by different diastereomers of the tag (Ikegami et al. 2004; Prudêncio et al. 2004; Pintacuda et al. 2004; Vlasie et al. 2007). The latter was a severe problem with some of the first generation tags (Leonov et al. 2005). In order to prevent these stereochemical problems we decided to synthesize a highly symmetric paramagnetic tag

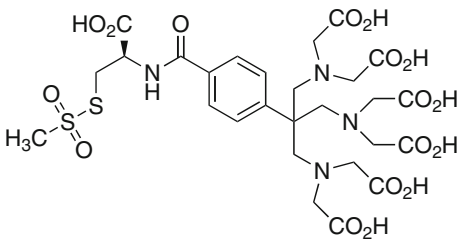


**Fig. 1** Structure of Cys-Ph-TAHA (cysteinyl-phenyl-triaminohexaacetate). The tag was synthesized in 7 steps with 28% total yield. The $C_3$-symmetric chelate function has a high affinity to lanthanide ions and allows for the precise measurement of RDCs

based on the TAHA chelator (Viguier et al. 2001; Arslantas et al. 2004). This $C_3$-symmetric ligand offers nine coordination sites and forms stable complexes with lanthanide ions (e.g. log K = 14.85 for $Dy^{3+}$ at pH 7, Viguier et al. 2001). As was determined by dysprosium induced shift measurements (Alpoim et al. 1992), less than 1.4 water molecules are located within the inner coordination sphere at pH 7.

## Experimental section

### Preparation of tagged ubiquitin

The protein was expressed recombinantly in *E. coli* and purified by established methods (Lazar et al. 1997; You et al. 1999). The tagging reaction was performed reproducibly in the following way: The tag was pre-loaded in deionized water with a twofold excess of $LnCl_3$. The aqueous stock solutions of Cys-Ph-TAHA (5 eq., c = 10 mg $mL^{-1}$) and $LnCl_3$ (10 eq., c = 10 mg $mL^{-1}$) were combined and incubated for 2.5 h at 20°C. The reduced, uniformly labelled protein ($^{15}N$ or $^{13}C$,$^{15}N$) was dissolved in 200 µL buffer (MOPS 50 mM, NaCl 50 mM, pH 8). Both solutions were combined and shaken at 20°C. After 75 min the reaction went to completion as monitored by ESI–MS spectrometry. The excess lanthanide ions ($Ln(OH)_3$) were removed by centrifugation, the supernatant transferred into a Vivaspin 2 concentrator (2 mL, PES membrane, 5000 MWCO) and the buffer was exchanged (10×) with the NMR buffer (MOPS 50 mM, NaCl 50 mM, pH 6.8) to remove excess of tag-bound lanthanides. Afterwards, the protein solution was transferred into a Shigemi tube and $D_2O$ (20 µL) was added.

Alternatively, the excess of $Ln^{3+}$ can be precipitated by addition of pH 8 buffer before combining of the tag solution with the protein solution.

### Production and tagging of LacR

The expression plasmid pET-LICHISΔOΔlacI-lac333 construct containing the dimeric Lac repressor mutant lac333K84 M was described previously (De Jong et al. 2006; Romanuka et al. 2009). This plasmid served as a template to generate LacR mutants containing one free Cys, while the other two natural Cys residues present in LacR were mutated to Ser or Ala using KOD polymerase (Novagen). Mutations were confirmed by DNA sequencing.

Overexpressions of the $^{2}H$ and $^{15}N$ labeled Lac333K84 M Cys mutants was achieved in BL21 (DE3) using an auto-induction medium (Studier 2005). The low amount of lactose present in the auto-induction medium combined with the low affinity of (allo)lactose for the Lac repressor

leads to the formation of unliganded Lac repressor after purification. Transformations, pre-culturing, growth and overexpressions were carried out as described previously (Romanuka et al. 2009). The final cell density was 6–7 at OD600. The harvested cells (500 mL culture) were resuspended in 15 mL lysis buffer containing 2 mM $\beta$-mercaptoethanol and frozen at −80°C. After sonication, the crude lysate was centrifugated at 15,000 rpm for 45 min at 4°C in a Sorvall SS34 rotor. The supernatant was loaded onto a 1.7 mL Nickel loaded POROS metal chelating affinity chromatography column (PerSeptive Biosystems). The column was subsequently washed with 30 column volumes of binding buffer (50 mM MOPS pH 8.0, 400 mM KCl, 20 mM imidazole, 1 mM PMSF) and protein was eluted using an isocratic elution in binding buffer containing 500 mM imidazole. To the eluted, protein-containing fraction MOPS, glycine and glycerol were immediately added to a final concentration of 1 M, 1.2 M and 5%, respectively, followed by immediate addition of 5 molar excess of Ln-preloaded Cys-Ph-TAHA. The protein concentration was adjusted to 0.1 mM in a 3 mL reaction mix. Completeness of the reaction was followed using Ellman's reagent (5,5′-dithiobis-(2-nitrobenzoic acid) or DTNB). At different time points 50 µL reaction aliquots were diluted to 1 mL in a binding buffer containing 0.1 mM DTNB. The absorbance at 412 nm was used to indicate the completeness of the reaction. When no absorbance increase was noted with respect to the binding buffer with 0.1 mM DTNB, all LacR Cys had reacted. To make the LacR-DNA complex, the palindromic 22 bp SymL *lac* operator was added in 1:1 molar ratio to the reaction mix. HPLC purified single-strand SymL DNA (5′-GAATTGTGAGCGCTCACAATTC-3′) was purchased from Eurogentec and from this double-strand DNA was prepared as described previously (Romanuka et al. 2009). Buffer exchange of the tagged protein-DNA complex to a degassed NMR buffer (50 mM MOPS pH 7.2, 1 M [U-$^2$H]-Gly, 5% [U-$^2$H]-glycerol, 10 mM KCl and 0.01% $NaN_3$) was performed on a 2 mL 7 K MWCO Zeba Spin desalting column (Thermo Scientific). Next a 30-fold molar excess of IPTG was added to form the ternary complex of LacR with DNA and IPTG.

The affinities of wt and tagged LacR for IPTG and operator were measured as described previously (Spronk et al. 1999; Xu and Matthews 2009).

## Protein NMR-spectroscopy

All protein NMR experiments, unless otherwise stated, were performed at 298 K. The $^1$H-$^{15}$N HSQC spectra for the PCS determination were measured on an 800 MHz Bruker AvanceIII spectrometer equipped with a TCI z-gradient cryoprobe. $^1$H-$^{15}$N IPAP-HSQC spectra (Ottiger et al. 1998) and $^1$H-$^{15}$N TROSY spectra were obtained on 900 MHz Bruker Avance spectrometers with TCI z-gradient cryoprobes. For the sequential assignment 3D $^1$H-$^{15}$N NOESY-HSQC (900 MHz) and HNCA spectra (800 MHz) were recorded. The spectra were processed with the nmrPipe package (Delaglio et al. 1995) and analyzed using the software packages SPARKY (Goddard and Kneller 2008) and CARA (Keller 2004).

## Evaluation of PCSs and RDCs

PCS and RDC data were evaluated with a series of in-house written MATLAB scripts, which are made available upon request. PCS (Table 1) and RDC (Table 2) tensors were calculated by a least squares fit of the experimental values to the protein coordinates. For all evaluations we used structural ensembles (1D3Z (Cornilescu et al. 1998), EROS (Lange et al. 2008), EROS II (unpublished results) and ERNST (Fenwick et al. 2011)), where the non-linear coordinate dependent terms (i.e. the terms describing the vector orientation and the $r^{-3}$ terms in the case of PCSs) were averaged for all conformers before the least squares fits were performed. In the PCSs evaluation, the metal position was

**Table 1** Overview of the obtained tensors from PCS data

| Sample | Q | $R^2$ | x | y | z | $\Delta\chi_{ax}$ | $\Delta\chi_{rh}$ | $\alpha$ | $\beta$ | $\gamma$ |
|---|---|---|---|---|---|---|---|---|---|---|
| T12C Tb | 0.18 | 0.97 | 35.7 | −77.0 | 5.0 | −14.83 | −2.51 | 141.8 | 92.7 | −23.0 |
| T12C Tm | 0.15 | 0.98 | 38.2 | −71.9 | 6.3 | −13.42 | −3.84 | 7.2 | 72.8 | 100.8 |
| T12C Tb* | 0.25 | 0.94 | 36.4 | −71.9 | 5.8 | 14.09 | 7.35 | −8.6 | 62.2 | 92.0 |
| T12C Tm* | 0.19 | 0.96 | 36.4 | −71.9 | 5.8 | −15.93 | −7.42 | 13.4 | 79.6 | 94.2 |
| S57C Tb | 0.07 | 0.99 | 59.7 | −91.7 | 12.0 | −12.71 | −8.28 | 19.4 | 98.1 | 158.3 |
| S57C Tm | 0.11 | 0.98 | 59.7 | −86.7 | 11.1 | 8.47 | 1.22 | −139.4 | 47.8 | −12.7 |
| S57C Tb* | 0.12 | 0.98 | 61.0 | −89.4 | 13.2 | −11.49 | −6.68 | 29.3 | 94.3 | 144.7 |
| S57C Tm* | 0.17 | 0.97 | 61.0 | −89.4 | 13.2 | 17.73 | 5.17 | −150.5 | 51.2 | 14.2 |

The metal coordinates x, y, z [Å] refer to the molecular frame. $\Delta\chi_{ax}$ and $\Delta\chi_{rh}$ are the axial and rhombic components of the $\chi$-tensor, respectively, $\alpha$, $\beta$, $\gamma$ are the Euler angles in z, y′, z″ notation, R is the correlation factor. Sets marked with an asterisk were fitted using a common metal position for $Tb^{3+}$ and $Tm^{3+}$. In all calculations, all conformations of the pdb file 1D3Z were fitted into a single tensor

**Table 2** Overview of the obtained tensors from RDC data

| Sample | Ensemble | Q | $R^2$ | $\Delta\chi_{ax}$ | $\Delta\chi_{rh}$ | $\alpha$ | $\beta$ | $\gamma$ |
|---|---|---|---|---|---|---|---|---|
| T12C Tb | 1D3Z | 0.12 | 0.99 | 14.38 | 1.64 | 134.0 | 94.2 | −74.4 |
| | EROS | 0.09 | 0.99 | 16.76 | 1.58 | 147.5 | 99.9 | −72.1 |
| | EROS II | 0.08 | 0.99 | 15.85 | 1.59 | 145.7 | 99.8 | −71.7 |
| | ERNST | 0.12 | 0.98 | 15.96 | 1.75 | 154.7 | 98.4 | −73.7 |
| T12C Tm | 1D3Z | 0.18 | 0.97 | 9.27 | 5.34 | 6.8 | 98.3 | 12.9 |
| | EROS | 0.15 | 0.98 | 11.05 | 5.86 | 12.5 | 96.5 | 16.2 |
| | EROS II | 0.15 | 0.98 | 10.44 | 5.44 | 12.7 | 96.4 | 16.3 |
| | ERNST | 0.17 | 0.97 | 10.85 | 5.14 | 11.4 | 94.7 | 14.4 |
| S57C Tb | 1D3Z | 0.17 | 0.96 | 5.91 | 3.75 | −10.4 | 59.0 | −112.5 |
| | EROS | 0.14 | 0.98 | 6.98 | 4.45 | −15.4 | 65.2 | −107.4 |
| | EROS II | 0.14 | 0.98 | 6.63 | 4.03 | −15.8 | 65.8 | −108.1 |
| | ERNST | 0.14 | 0.98 | 6.77 | 4.44 | −12.0 | 66.4 | −111.0 |
| S57C Tm | 1D3Z | 0.26 | 0.93 | 5.69 | 1.23 | −133.9 | 54.2 | −18.1 |
| | EROS | 0.30 | 0.91 | 7.32 | 1.79 | −126.6 | 58.2 | −20.4 |
| | EROS II | 0.33 | 0.90 | 6.74 | 1.61 | −129.0 | 56.9 | −21.2 |
| | ERNST | 0.34 | 0.89 | 6.90 | 1.68 | −125.2 | 56.0 | −22.2 |

$\Delta\chi_{ax}$ and $\Delta\chi_{rh}$ are the axial and rhombic components of the $\chi$-tensor, respectively, $\alpha$, $\beta$, $\gamma$ are the Euler angles in z, y′, z″ notation, $R$ is the correlation factor. In all calculations, all conformations of the respective ensemble were fitted into a single tensor. The RDCs were also scaled with $S^{overall} = 0.93$ and fitted against the EROS, EROS II and ERNST ensembles instead of 1D3Z

determined using a grid search algorithm, until the metal coordinates that provided the smallest $Q$-factor were found.

## Results

The structure of Cys-Ph-TAHA is shown in Fig. 1. Starting from commercially available materials, Cys-Ph-TAHA was synthesized in 7 steps with a total yield of 28% after HPLC purification. The experimental details are given in the supporting information (Scheme S1). Due to the simple design without stereogenic centers on the chelator itself, Cys-Ph-TAHA can be easily produced on a scale of a few hundred milligrams.

At first we tagged ubiquitin, which is an excellent model system for NMR spectroscopy. With the protocol described in the materials and methods section, the pre-loaded tag can be attached efficiently to the protein. We used two different mutants (T12C and S57C) and tagged them with $Tb^{3+}$- and $Tm^{3+}$-loaded Cys-Ph-TAHA, which gave a total of four anisotropic samples. In the following they are abbreviated by the mutant and the lanthanide ion (e.g. T12C Tb). Additionally, $Lu^{3+}$-loaded diamagnetic reference samples were produced. In all four paramagnetic ubiquitin samples the majority of the NMR signal remained sharp (Fig. 1), which indicates very small amounts of free lanthanide ions in solution. Some resonances near the paramagnetic tag were broadened even beyond detection due to paramagnetic relaxation (Tables S1, S2).

### PCSs and RDCs

HSQC spectra for the PCS measurements were recorded at 18.8 T and 298 K. Figure 2 shows an overlay of the $^{1}H$-$^{15}N$ HSQC spectra of T12C Tm and T12C Lu. Compared to the isotropic sample, only five resonances were broadened beyond detection due to the paramagnetic relaxation enhancement. The backbone amide signals of all anisotropic samples were sequentially assigned using 3D HNCA and 3D $^{1}H$-$^{15}N$ NOESY-HSQC spectra. Large PCSs up to 2 ppm (Tables S1, S2) were observed and used in conjunction with the NMR structure of ubiquitin (pdb code 1D3Z, Cornilescu et al. 1998) to calculate the magnetic susceptibility tensors for each sample using a single tensor for all 10 structures. The back-calculated PCSs are in excellent agreement with the experimental ones (Fig. 3). This is reflected by the small $Q$-factors that are between 0.07 and 0.18 for all data sets (Table 1). In agreement with previously reported tensors (Bertini et al. 2001) the PCS patterns for terbium and thulium are opposite in sign but otherwise similar, yet not identical. The metal positions found for T12C Tb and T12C Tm are about 5 Å away from each other. Similar results had been observed previously (Su et al. 2008a), and had been attributed to the inaccuracy in the evaluation of the metal position and the $\Delta\chi$ tensor when working with flexible tags. In order to obtain a metal position in agreement with both data sets, we fitted the tensors again using a common position for $Tb^{3+}$ and $Tm^{3+}$, which did not reduce the quality of the fit considerably (Table 1; Fig. 3).

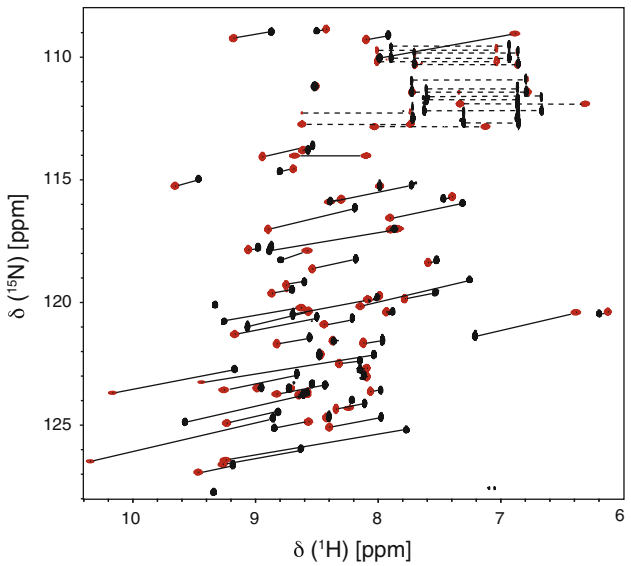


**Fig. 2** $^{1}$H-$^{15}$N HSQC spectra (18.8 T, 800 MHz, 298 K) for Cys-Ph-TAHA-tagged ubiquitin-T12C loaded with diamagnetic lutetium (T12C Lu, *black*) and paramagnetic thulium (T12C Tm, red). Aliased peaks (States-TPPI) are not shown but the chemical shifts are listed in Table S1. A total of 65 PCSs, indicated by the *black lines*, were extracted from the spectra. The *dashed lines* connect side chain signals

We investigated the temperature stability of the tag with respect to additional signal sets observed in the spectra. This was triggered by the observation that for the DOTA-M8 tag a second, temperature dependent species was found (Häussinger et al. 2009). This species had a molar fraction of 15–20% at 298 K and up to 50% at 323 K. With both lanthanide ions in the T12C mutant the Cys-Ph-TAHA tag showed two minor sets of peaks for some residues with a molar ratio of approximately 2%. These additional peaks are shifted in relation to the major anisotropic and isotropic peaks. We tested the temperature behaviour for Cys-Ph-TAHA in a range from 278 to 315 K and observed that the populations of these minor anisotropic species remained constant within this temperature range (Fig. 4). Furthermore, remaining signals from the isotropic protein account for no more than 2% of the intensity as compared to the anisotropic peaks for the T12C mutant. Interestingly, these additional peaks were not observed for the S57C mutant neither at 278 K nor at 315 K. The origin of these signals remains unclear. However, since they are only visible for one mutant we assume that they arise by slow conformational averaging at the linker between the protein and the tag. The temperature dependent chemical shift changes of these additional peaks reflect the temperature dependence of both the isotropic chemical shift and the pseudocontact shift. As expected, the size of the PCSs increases at lower temperatures due to a tensor scaling reflecting the $T^{-2}$ dependence of the PCSs (McGarvey 1979). Hence, the calculated metal positions over the applied temperature range of 37 K are very similar (Figure S1). It is important to note that the increase in temperature did not lead to any decomposition of the tag (Figure S2).

Since the lanthanide-loaded tag aligns the protein, we measured RDCs at 21.1 T and 298 K. After exclusion of

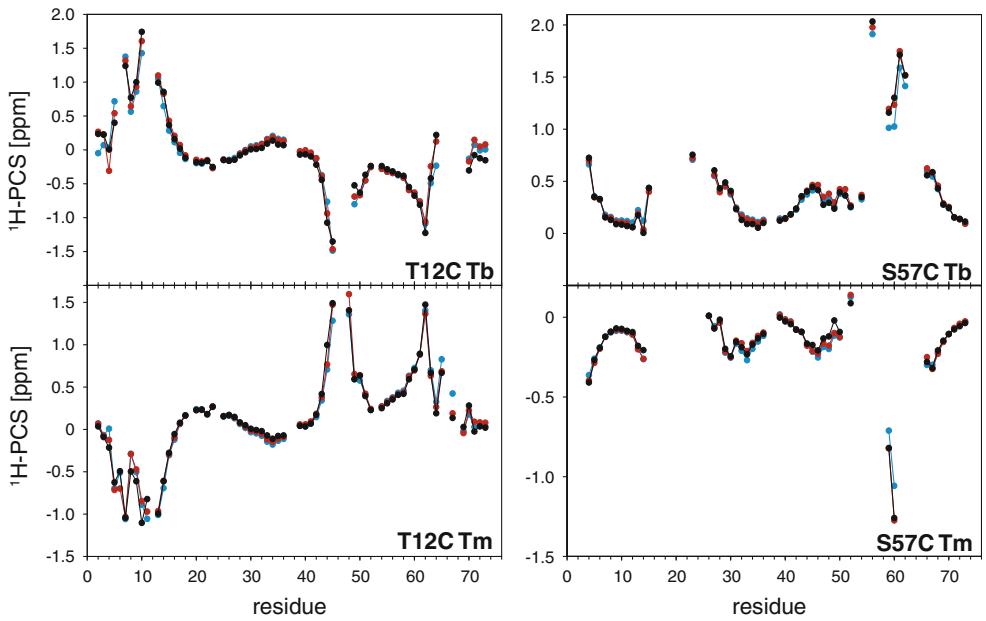


**Fig. 3** Comparison of the experimental (*black*) and the back-calculated (*red*) $^{1}$H-PCSs of the four anisotropic samples. In addition, the back-calculated $^{1}$H-PCSs using a common metal position for $Tb^{3+}$ and $Tm^{3+}$ are shown (*blue*). All calculations used a single tensor for all 10 structures (1D3Z) and the results are given in Table 1. The mobile residues R74–G76 were excluded from the calculations. The chemical shifts and resulting PCSs are listed in the Tables S1, S2

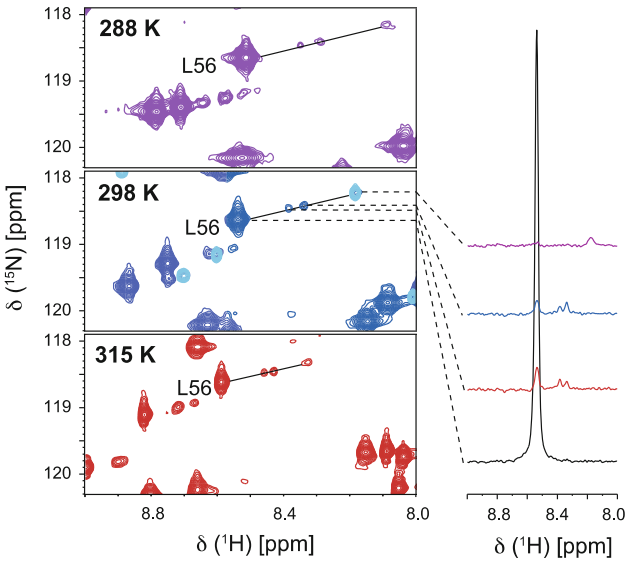


**Fig. 4** Sections of the $^{1}H,^{15}N$ HSQC spectra from Cys-Ph-TAHA tagged ubiquitin-T12C, loaded with thulium at different temperatures. The spectrum at 298 K is overlaid with the diamagnetic reference (*light blue*). The spectra are displayed at low contour level. For L56, the 1D-traces, all plotted at the same noise level, are shown representatively. The relative population of the minor peaks is not increasing within the temperature range of 278 to 315 K

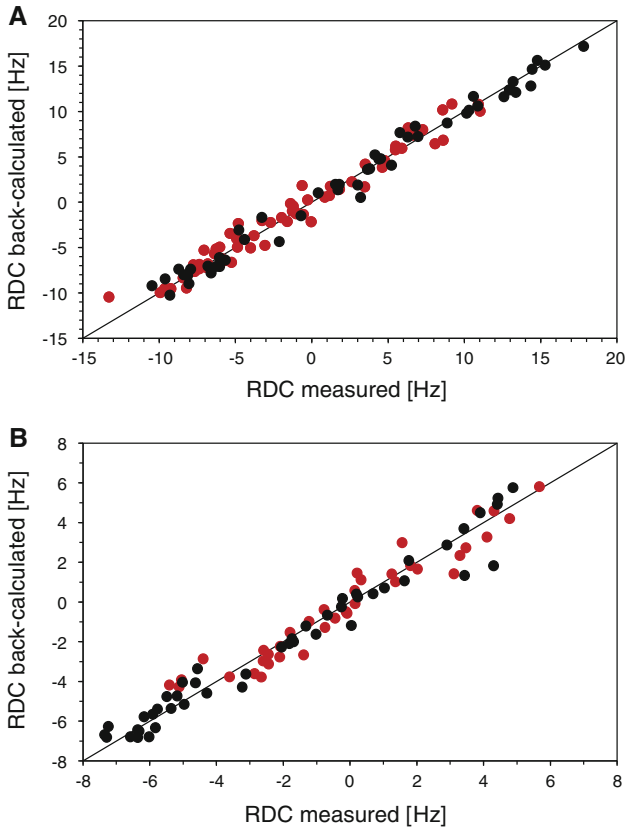


**Fig. 5** Comparison of the measured and back-calculated RDCs using a single tensor for all 10 structures from the pdb file (1D3Z). **a** Shows data from T12C Tb (black) and T12C Tm (*red*), **b** from S57C Tb (*black*) and S57C Tm (*red*). The tensors are given in Table 1. RDCs were measured at 21.1 T and 298 K. The experimental RDCs are listed in the Tables S1, S2

the flexible C-terminal residues (R74–G76) as well as those residues displaying either very broad or overlapped signals in the IPAP spectrum, a large number of RDCs remained for further evaluation. In the case of the T12C mutant, we obtained large RDCs up to 18 Hz while the maximum RDC measured for the S57C mutant was 8 Hz. We attribute these smaller RDCs to higher flexibility of the tag when attached to the S57C mutant. This enhanced flexibility is in good agreement with the fact that more residues are bleached for S57C than for T12C.

In addition to tag mobility, anisotropic parameters are also affected by internal mobility of the protein. Therefore, in analogy to the calculation of the PCSs, we fitted the RDCs into a single tensor using all 10 structures of the 1D3Z ensemble in order to provide a more accurate description of conformational average. The correlation plots are shown in Fig. 5. Especially for T12C, the experimental RDCs provided excellent fits as reflected by *Q*-factors of 0.12 (T12C Tb) and 0.18 (T12C Tm). If calculated for a single structure, the *Q*-factors can be even lower (i.e. for the first structure of 1D3Z we obtained *Q*-factors of 0.08 and 0.13, respectively (data not shown). The tensors fitting these RDCs, however, have smaller axial components than the PCS derived tensors. Since RDCs are more sensitive to motions than PCSs we investigated how much the RDC-derived tensors change taking internal protein motion into account. For this purpose we based the tensor back-calculation on the previously determined ubiquitin ensembles EROS (Lange et al. 2008), EROS II (unpublished results) and ERNST (Fenwick et al. 2011), which reflect supra-$\tau_c$ motion of the protein backbone. Since these ensembles do not take into account the overall scaling of the order parameters due to fast motion, we divided the RDCs by the overall scaling factor $S^{overall} = 0.93$ and fitted against these ensembles (Table 2). It has been shown from a recently derived solid-state NMR study on ubiquitin, that this scaling factor is conservative (Schanda et al. 2010). The obtained *Q*-factors are generally lower than for the 1D3Z ensemble and the tensor magnitude increases by approximately 15–20% as expected. However, we still found smaller RDC tensors than PCS tensors for T12C Tm, S57C Tb and S57C Tm. The observation that RDC derived tensors are in general smaller than PCS derived tensors is not new and has been previously reported with other tags. This has been attributed to different susceptibility of PCSs and RDCs to motions of the tag (Su et al. 2008a; Keizers et al. 2008; Häussinger et al. 2009) and will be further investigated in a separate study describing the motion of the tag.

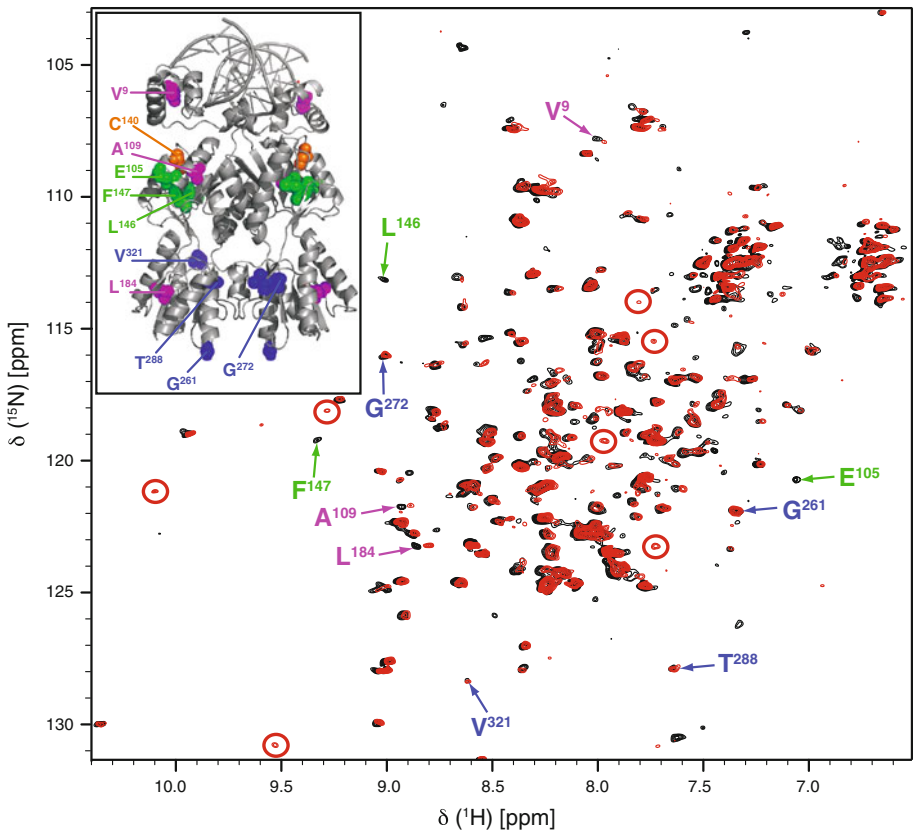


**Fig. 6** $^{1}$H-$^{15}$N TROSY spectra (21.1 T, 900 MHz, 317 K) of Cys-Ph-TAHA-tagged LacR dimer loaded with diamagnetic lutetium (*black*) and paramagnetic thulium (*red*) in a ternary complex with a symmetric operator and IPTG and the X-ray structure of LacR bound to the O2 operator (pdb code 1EFA) in the *upper* left panel. The position of the tagged Cys is marked in orange in the X-ray structure. Exemplary, signals most evidently arising from PCSs are indicated by *red circles*. Residues marked in blue were not affected by the paramagnetic thulium and are at a distance from 35 to 55 Å from the tagged Cys, residues marked in *green* are within 10 Å from the tagged Cys and bleached in the paramagnetic spectra, while residues marked in *purple* (between 10 and 35 Å from the tagged Cys) show small PCSs

Tagging of LacR

To investigate whether the Cys-Ph-TAHA tag can also be used for more biochemically challenging proteins, we tagged a fully deuterated, $^{15}$N-labelled dimeric Lac repressor (LacR, residues 1–333) in a 90 kD ternary complex (bound to DNA and IPTG). LacR contains three free cysteine residues at positions 107, 140 and 281. We attached Cys-Ph-TAHA to Cys140, while the other Cys residues were mutated to Ser or Ala, respectively. Tagged LacR was fully functional and thus able to bind ligands with the same binding constants as the wt LacR (data not shown). Importantly also, the tagging did not reduce solubility of LacR. In Fig. 6, the superimposed $^{1}$H-$^{15}$N TROSY-spectra (21.1 T, 317 K) of the tagged LacR, loaded with lutetium and thulium, respectively, are shown. Although the anisotropic spectrum has not been completely assigned up to now (which will be communicated elsewhere), some qualitative statements can be made. The spectrum features some significant PCSs in addition to small PCSs for other residues. In the paramagnetic spectrum, there are two peaks at 9.53/130.8 and 10.15/121.2 ppm ($^{1}$H/$^{15}$N). In the diamagnetic spectrum, there are no peaks in this region. The closest are around 9 ppm. There are two possibilities: The diamagnetic peak is broadened because of some exchange processes. This would require that tagging would slow down or remove these processes, which is pretty unlikely. The other explanation that we think is reasonable is that the diamagnetic peaks are visible indicating that the proton PCS must be at least 1 ppm (for the 10.15 ppm peak) and 0.5 ppm for the (9.53 ppm) peak. The size of these PCSs (up to 1 ppm at 317 K) seems reasonable compared to the PCSs observed for ubiquitin at 315 K (data not shown).

The observed paramagnetic effects are in agreement with the X-ray structure as indicated by some exemplarily chosen residues that could be assigned. Since the LacR occurs as a dimer, the observed paramagnetic effects are distance weighted tensorial sums induced by the two paramagnetic centers. To obtain the shown spectral quality, measurements had to be done at 317 K over an extended amount of time (e.g. 27 h for the paramagnetic sample). Even after two weeks, the spectrum did not show any changes. This provides evidence for the pronounced temperature stability of the attached Cys-Ph-TAHA and demonstrates also that Cys-Ph-TAHA has a much higher affinity for lanthanides than DNA.

## Conclusions

We have presented Cys-Ph-TAHA, a new paramagnetic tag based on the nonadentate TAHA ligand. Cys-Ph-TAHA is

easy to synthesize and can be attached efficiently to a single cysteine residue. Using the described simple tagging protocol we obtained reproducible paramagnetic samples that provided spectra with excellent line widths allowing for the accurate measurement of large PCSs and RDCs. Good fits to the NMR structure of ubiquitin and even better ones to ubiquitin ensembles confirmed the high quality of these data sets. The PCS and RDC derived tensors do not agree completely due to the dynamics of the tag, which will be investigated in a future work.

The obtained spectra did not show any significant contribution of additional anisotropic species. The Cys-Ph-TAHA tag displays a femtomolar metal affinity (Viguier et al. 2001) and excellent thermal stability in the temperature range between 278 and 315 K or greater. This is an interesting feature especially for studies of thermophilic proteins and might be a unique feature of this tag. For elevated temperatures no data has been reported for the two-point attached tags such as CLaNP-5, and large contributions of a second anisotropic species have been reported for the DOTA-M8-tag. However, the Cys-Ph-TAHA tag is pH sensitive and will not be useful for studies at a pH lower than 4 and can therefore not be used for the study of pH induced unfolded proteins or their molten globules. The tag also leads to smaller susceptibility tensors than CLaNP-5 or the DOTA-M8 tag. However, its chemical availability, simplicity of application and stereochemical uniformity in combination with the pronounced thermal and chemical stability and high metal affinity make Cys-Ph-TAHA an interesting new tag. The tag could be attached also to a biochemically challenging ternary protein-DNA complex. Successful tagging and loading of the LacR dimer in the ternary complex raises the hope that Cys-Ph-TAHA may prove to be an excellent tool for paramagnetic NMR spectroscopy.

**Acknowledgments** This work was supported by the Max Planck Society (to C.G.), the Netherlands Foundation for Scientific Research (NWO-CW, to R.B.) and by the European Union (Bio-NMR project 261863, to C.G. and R.B., and East-NMR project 228461, to R.B.). We thank Karin Giller for the expression and purification of the ubiquitin mutants, Dr. Gert Folkers for support in expression and purification of the Lac repressor mutants, Gerhard Wolf, Kerstin Overkamp for HPLC purifications and mass spectrometry, Jens Schimpfhauser for the large-scale synthesis, Prof. Dr. Markus Zweckstetter, Dr. Donghan Lee, Dr. Edward d'Auvergne, David Ban, Dr. Holger Schmidt, Dr. Gert Folkers and Dr. Hans Wienk for assistance and fruitful discussions, David Ban for careful reading of the manuscript and Dr. Holm Frauendorf from the Institute of Organic and Biomolecular Chemistry of the University of Göttingen for the acquisition of HRMS spectra.



## References

Allegrozzi M, Bertini I, Janik MBL, Lee G, Liu YM, Luchinat C (2000) Lanthanide- induced pseudocontact shifts for solution structure refinements of macromolecules in shells up to 40 Å from the metal ion. J Am Chem Soc 122:4154–4161

Alpoim MC, Urbano AM, Geraldes CFGC, Peters JA (1992) Determination of the number of inner-sphere water molecules in lanthanide(III) polyaminocarboxylate complexes. J Chem Soc Dalton Trans 1992:463–467

Arslantas E, Smith-Jones PM, Ritter G, Schmidt RR (2004) TAME-Hex A - a novel bifunctional chelating agent for radioimmunoimaging. Eur J Org Chem 19:3979–3984

Barthelmes K, Reynolds A, Peizach E, Jonker HRA, Denunzio N, Allen K, Imperiali B, Schwalbe H (2011) Engineering encodable lanthanide-binding tags (LBTs) into loop regions of proteins. J Am Chem Soc 133:808–819

Bertini I, Luchinat C (1999) New applications of paramagnetic NMR in chemical biology. Curr Opin Chem Biol 3:145–151

Bertini I, Janik MBL, Lee YM, Luchinat C, Rosato A (2001) Magnetic susceptibility tensor anisotropies for a lanthanide ion series in a fixed protein matrix. J Am Chem Soc 123:4181–4188

Bertini I, Luchinat C, Parigi G (2002) Magnetic susceptibility in paramagnetic NMR. Prog Nucl Magn Res Spec 40:249–273

Bertini I, Gelis I, Katsaros N, Luchinat C, Provenzani A (2003) Tuning the affinity for lanthanides of calcium binding proteins. Biochemistry 42:8011–8021

Cornilescu G, Marquardt JL, Ottiger M, Bax A (1998) Validation of protein structure from anisotropic carbonyl chemical shifts in a dilute liquid crystalline phase. J Am Chem Soc 120:6836–6837

De Jong RN, Daniels MA, Kaptein R, Folkers GE (2006) Enzyme free cloning for high throughput gene cloning and expression. J Struct Funct Genom 7:109–118

Delaglio F, Grzesiek S, Vuister GW, Zhu G, Pfeifer J, Bax A (1995) NMR-Pipe: a multidimensional spectral processing system based on UNIX pipes. J Biomol NMR 6:277–293

Fenwick RB, Esteban-Martin S, Richter B, Lee D, Walter KFA, Milovanovic D, Becker S, Lakomek NA, Griesinger C, Salvatella X (2011) Weak long-range correlated motions in a surface patch of ubiquitin involved in molecular recognition. J Am Chem Soc 133:10336–10339

Gaponenko V, Altieri AS, Li J, Byrd A (2002) Breaking symmetry in the structure determination of (large) symmetric protein dimers. J Biomol NMR 24:143–148

Goddard TD, Kneller DG (2008) Sparky 3. University of California, San Francisco

Haberz P, Rodriguez-Castañeda F, Junker J, Becker S, Leonov A, Griesinger C (2006) Two new chiral EDTA-based metal chelates for weak alignment of proteins in solution. Org Lett 8:1275–1278

Häussinger D, Huang JR, Grzesiek S (2009) DOTA-M8: An extremely rigid, high- affinity lanthanide chelating tag for PCS NMR spectroscopy. J Am Chem Soc 131:14761–14767

Hus JC, Marion D, Blackledge M (2000) De novo determination of protein structure by NMR using orientational and long-range order restraints. J Mol Biol 298:927–936

Ikegami T, Verdier L, Sakhaii P, Grimme S, Pescatore B, Saxena K, Fiebig KM, Griesinger C (2004) Novel techniques for weak alignment of proteins in solution using chemical tags coordinating lanthanide ions. J Biomol NMR 29:339–349

Keizers PHJ, Desreux JF, Overhand M, Ubbink M (2007) Increased paramagnetic effect of a lanthanide protein probe by two-point attachment. J Am Chem Soc 129:9292–9293

Keizers PHJ, Saragliadis A, Hiruma Y, Overhand M, Ubbink M (2008) Design, synthesis, and evaluation of a lanthanide chelating protein

probe: CLaNP-5 yields predictable paramagnetic effects independent of environment. J Am Chem Soc 130:14802–14812
Keller RLJ (2004) Optimizing the process of nuclear magnetic resonance spectrum analysis and computer aided resonance assignment. Dissertation, Swiss Federal Institute of Technology, Zürich
Kramer F, Deshmukh MV, Kessler H, Glaser SJ (2004) Residual dipolar coupling constants: an elementary derivation of key equations. Concepts Magn Res Part A 21:10–21
Lakomek NA, Carlomagno T, Becker S, Griesinger C, Meiler J (2006) A thorough dynamic interpretation of residual dipolar couplings in ubiquitin. J Biomol NMR 34:101–115
Lakomek NA, Lange OF, Walter KFA, Farès C, Egger D, Lunkenheimer P, Meiler J, Grubmüller H, Becker S, de Groot BL, Griesinger C (2008) Residual dipolar couplings as a tool to study molecular recognition of ubiquitin. Biochem Soc Trans 36: 1433–1437
Lange OF, Lakomek NA, Farès C, Schröder GF, Walter KFA, Becker S, Meiler J, Grubmüller H, Griesinger C, de Groot BL (2008) Recognition dynamics up to microseconds revealed from an RDC-derived ubiquitin ensemble in solution. Science 320:1471–1475
Lazar GA, Desjarlais JR, Handel TM (1997) De novo design of the hydrophobic core of ubiquitin. Protein Sci 6:1167–1178
Leonov A, Voigt B, Rodriguez-Castañeda F, Sakhaii P, Griesinger C (2005) Convenient synthesis of multifunctional EDTA-based chiral metal chelates substituted with an *S*-mesylcysteine. Chemistry 11:3342–3348
Man B, Su XC, Liang H, Simonsen S, Huber T, Messerle BA, Otting G (2010) 3- Mercapto-2, 6-pyridinedicarboxylic acid: a small lanthanide-binding tag for protein studies by NMR spectroscopy. Chem Eur J 16:3827–3832
Martin LJ, Hähnke MJ, Nitz M, Wöhnert J, Silvaggi NR, Allen KN, Schwalbe H, Imperiali B (2007) Double-lanthanide-binding tags: design, photophysical properties, and NMR applications. J Am Chem Soc 129:7106–7113
McGarvey BR (1979) Temperature dependence of the pseudocontact shift in lanthanide shift reagents. J Magn Res 33:445–455
Nitz M, Sherawat M, Franz KJ, Peisach E, Allen KN, Imperiali B (2004) Structural origin of the high affinity of a chemically evolved lanthanide-binding peptide. Angew Chem Int Ed 43: 3682–3685
Ottiger M, Delaglio F, Bax A (1998) Measurement of *J* and dipolar couplings from simplified two-dimensional NMR spectra. J Magn Reson 131:373–378
Otting G (2008) Prospects for lanthanides in structural biology by NMR. J Biomol NMR 42:1–9
Pintacuda G, Moshref A, Leonchiks A, Sharipo A, Otting G (2004) Site-specific labelling with a metal chelator for protein-structure refinement. J Biomol NMR 29:351–361
Prudêncio M, Rohovec J, Peters JA, Tocheva E, Boulanger MJ, Murphy MEP, Hupkes HJ, Kosters W, Impagliazzo A, Ubbink M (2004) A caged lanthanide complex as a paramagnetic shift agent for protein NMR. Chem Eur J 10:3252–3260
Rodriguez-Castañeda F, Haberz P, Leonov A, Griesinger C (2006) Paramagnetic tagging of diamagnetic proteins for solution NMR. Magn Reson Chem 44:10–16
Romanuka J, van den Bulke H, Kaptein R, Boelens R, Folkers GE (2009) Novel strategies to overcome expression problems encountered with toxic proteins: application to the production of Lac repressor proteins for NMR studies. Protein Expr Purif 67:104–112
Schanda P, Meier BH, Ernst M (2010) Quantitative analysis of protein backbone dynamics in microcrystalline ubiquitin by solid-state NMR spectroscopy. J Am Chem Soc 132:15957–15967
Spronk CAEM, Folkers GE, Noordman AGW, Wechselberger R, van den Brink N, Boelens R, Kaptein R (1999) Hinge-helix formation and DNA bending in various *lac* repressor–operator complexes. The EMBO J 22:6472–6480
Studier FW (2005) Protein production by auto-induction in high-density shaking cultures. Protein Expr Purif 41:207–234
Su XC, Otting G (2010) Paramagnetic labelling of proteins and oligonucleotides for NMR. J Biomol NMR 46:101–112
Su XC, McAndrew K, Huber T, Otting G (2008a) Lanthanide-binding peptides for NMR measurements of residual dipolar couplings and paramagnetic effects from multiple angles. J Am Chem Soc 130:1681–1687
Su XC, Man B, Beeren S, Liang H, Simonsen S, Schmitz C, Huber T, Messerle BA, Otting G (2008b) A dipicolinic acid tag for rigid lanthanide tagging of proteins and paramagnetic NMR spectroscopy. J Am Chem Soc 130:10486–10487
Swarbrick JD, Ung P, Chhabra S, Graham B (2011a) An iminodiacetic acid based lanthanide binding tag for paramagnetic exchange NMR spectroscopy. Angew Chem Int Ed 50:4403–4406
Swarbrick JD, Ung P, Su XC, Maleckis A, Chhabra S, Huber T, Otting G, Graham B (2011b) Engineering of a bis-chelator motif into a protein $\alpha$-helix for rigid lanthanide binding and paramagnetic NMR spectroscopy. Chem Commun 47:7368–7370
Tolman JR, Flanagan JM, Kennedy MA, Prestegard JH (1995) Nuclear magnetic dipole interactions in field-oriented proteins: information for structure determination in solution. Proc Natl Acad Sci USA 92:9279–9283
Viguier R, Serratrice G, Dupraz A, Dupuy C (2001) New polypodal polycarboxylic ligands - complexation of rare-earth ions in aqueous solution. Eur J Inorg Chem 7:1789–1795
Vlasie MD, Comuzzi C, van den Nieuwendijk AMCH, Prudêncio M, Overhand M, Ubbink M (2007) Long-range-distance NMR effects in a protein labeled with a lanthanide-DOTA chelate. Chem Eur J 13:1715–1723
Wöhnert J, Franz KJ, Nitz M, Imperiali B, Schwalbe H (2003) Protein alignment by a coexpressed lanthanide-binding tag for the measurement of residual dipolar couplings. J Am Chem Soc 125:13338–13339
Xu J, Matthews KS (2009) Flexibility in the inducer binding region is crucial for allostery in *Escherichia coli* lactose repressor. Biochemistry 48:4988–4998
Xu X, Keizers PHJ, Reinle W, Hannemann F, Bernhardt R, Ubbink M (2009) Intermolecular dynamics studied by paramagnetic tagging. J Biomol NMR 43:247–254
You J, Cohen RE, Pickart CM (1999) Construct for high-level expression and low misincorporation of lysine for arginine during expression of pET-encoded eukaryotic proteins in *Escherichia coli*. Biotechniques 27:950–954